Theoretical Considerations for Granular Flow

Thomas C. HALSEY
ExxonMobil Upstream Research Company
3120 Buffalo Speedway
Houston, TX 77098 USA

1 Introduction

Flows of hard granular systems are ubiquitous in nature and technology, yet are still poorly understood. Compared to truly microscopic dynamical or statistical mechanical systems, an unusual feature of granular systems is that they are intrinsically frictional and dissipative. Not only can dissipation arise through inelastic collisions between the particles, but also from frictional sliding between smooth or rough grain surfaces.

In the quasi-static "critical state" regime [1], the strain rates are smaller than any time scale of the system. One would expect deformations in this regime to be predominantly plastic in nature, corresponding to relatively long-lived particle contacts on the time scale $\dot{\gamma}^{-1}$. Beyond this regime, there appears to be a "dense granular flow" regime, marked by strain rates obeying

$$\sqrt{P/\rho_g L^2} < \dot{\gamma} < \sqrt{P/\rho_g d^2}, \tag{1}$$

with P the pressure, ρ_g the density, L a characteristic flow scale, and d the grain diameter. It is suspected that this regime has a rheology that distinguishes it from a higher strain-rate regime, in which

$$\dot{\gamma} > \sqrt{P/\rho_g d^2}. \tag{2}$$

This higher-strain rate regime seems to be appropriately described by kinetic-theory based studies [2].

The degree to which such studies can be extended into the dense granular flow regime defined by Eq. (1) remains controversial. A number of authors have claimed that key aspects of the rheology of dense granular flow can be recovered within kinetic theory treatments that include particle inelasticity and interparticle friction [3]. Halsey and Ertaş, and Jenkins, have posited the appearance of coherent structures in dense granular flows, which are difficult to reconcile with the underlying assumptions of kinetic theories [4, 5]. A significant work by the group author GDR MiDi pointed out that much of the phenomenology of dense granular flows can be organized using the "Inertia Number" [6]

$$I \equiv d\dot{\gamma}/\sqrt{P/\rho_g}. \tag{3}$$

An interesting feature of these results is the anomalously large fluctuations in the grain velocities, which scale with I in the dense flow regime,

$$\frac{\langle (\vec{v}(\vec{x}) - \langle \vec{v}(\vec{x}) \rangle)^2 \rangle}{(\dot{\gamma} d)^2} \sim I^{-\chi}, \tag{4}$$

where in dimensionalities $D = 2, 3$, $\chi \approx 1$ [6, 7]. Setting

$$I \equiv d/\ell, \tag{5}$$

defines the scale ℓ of the coherent structures hypothesized by Halsey and Ertaş.

The motivation to consider the dimensionless parameter I as a ratio of the particle diameter and a "mesoscopic" length scale ℓ arises from the overall phase diagram of flow on an incline. The dominant observational fact about the steady-state incline flows is the "Pouliquen flow rule," which connects the average velocity u of a flow of height h with the height $h_{stop}(\theta)$ at which flow ceases for a chute of inclination θ [8]. [The angle of repose $\theta_{\mathcal{R}}(h)$ is the inverse of the function $h_{stop}(\theta)$.] The Pouliquen flow rule gives a scaling form for u,

$$\frac{u}{\sqrt{gh}} = F(\frac{h}{h_{stop}}), \tag{6}$$

with g the gravitational acceleration, and where the function $F(x) \approx 0.136x$ for glass beads, and has a similar linear form for other types of particles [8, 9, 10].

The scaling $u \propto h^{3/2}$ in the Pouliquen flow rule is consistent with the classical Bagnold rheology [11]. But the Pouliquen flow rule also connects the coefficient of this proportionality, $u = A_{\mathrm{Bag}}(\theta)h^{3/2}$ with *the thickness of the pile at that inclination below which flow arrests*. Halsey and Ertaş have pointed out that this feature of the Pouliquen flow rule follows from the dependence of the rheology on I if it is assumed that flow arrests for thicknesses less than $h_{stop} \sim d/I = \ell$ [4]. Although Halsey and Ertaş proposed that this length scale corresponded to large-scale "eddy" structures in the flow, such eddies have proven elusive; a direct attempt to measure ℓ by measuring velocity correlations in flows was not successful [7].

The broad features of Pouliquen's conclusions have been confirmed by a series of numerical studies [9]. For relatively thin piles, the Bagnold rheology breaks down, but the thicker piles show a Bagnold rheology and obey the Pouliquen flow rule, albeit with a slightly larger value of β (The crossover is examined numerically in [12]). Although at large but not enormous values of particle stiffness, instantaneous coordination numbers are high (unlike in kinetic theory treatments), the duration of two-body collisions is still short compared to inverse strain rates $\dot{\gamma}^{-1}$ [13]. The density in the interior of the piles is independent of depth.

In this article I turn to the role of friction at enduring contacts in plastic flows. Of course, assuming that such long-lived contacts persist into the dense granular flow regime is problematic, due to the considerations regarding the short duration of two-body collisions mentioned above. To extend the conclusions of this work into this regime will require that the correlations characteristic of plastic flow with rolling and sliding contacts survive in a regime of frequent, albeit short, collisions between any particle and its neighbors. This would imply that a full theoretical description of this regime will require a synthesis of plastic flow and kinetic theory concepts.

Provided that the microscopic coefficient of friction μ defining the maximum value of the tangential force T at a contact divided by the normal force N is appreciable, we would anticipate that a significant fraction of long-lived contacts in a

deforming granular packing will be rolling as opposed to sliding. Simple counting of the number of constraints vs the number of variables indicates that states in which all contacts are rolling are not possible at coordination numbers $Z_c > 3$ for $D = 2$ or $Z_c > 4$ for $D = 4$. These results are simple extensions to the dynamical case of the famous isostatic criteria for static packings [14].

An interesting soluble case in $D = 2$ is presented by the honeycomb lattice, for which all particles have a coordination number $Z_c = 3$ exactly. This allows for a general solution of all states obeying the rolling constraint, corresponding to a full solution of the kinematics for this packing, in the limit $\mu \to \infty$, over times short enough that collisions do not degrade the lattice. It is also possible to solve exactly for both the tangential and normal forces exerted between the particles in this lattice; I present this explicitly for a particularly symmetric case of motion.

A striking feature of the kinematic solution is that even if the overall shear remains moderate, the rotational velocities of the particles are quite large. For a region of the packing of size ℓ with a constant shear $\dot{\gamma}$, the typical rotational velocity of the particles is $\omega \sim \dot{\gamma}\ell/d$. In addition, forces develop that limit the size of these regions of constant shear to

$$\ell < \frac{\sqrt{P/\rho_g}}{\dot{\gamma}}, \tag{7}$$

due to the requirement that all normal forces remain compressive. (Dry granular packings are unable to support tensions between the particles.) Equation (7) corresponds to the definition of the coherent structure size ℓ given in Eqs. (3,5) above.

Turning to disordered lattices, we see that the rotations arise from an underlying short-ranged anti-ferromagnetic ordering in the rotational velocities of the individual grains. This short-ranged ordering is frustrated by the existence in disordered lattices of odd plaquettes with odd numbers of links around the plaquette. In fact, it follows that it is not possible, even for quite large values of the coefficient of friction, for all of the particle contacts in a lattice with odd plaquettes to be rolling contacts. However, if sliding contacts are allowed, such that every odd plaquette has at least one sliding contact, then the remaining contacts can be rolling contacts; results on spin glasses then imply that it is possible that long-range ordered antiferromagnetic "spin-glass" regions will form. Of course, given the lack of direct correspondence between a statistical mechanical model (spin glasses) and a driven dissipative non-equilibrium system, it is not possible to draw rigorous conclusions from this analogy.

The remainder of this article is divided into 4 sections. In Section 2, we derive the critical coordination numbers for rolling states, and we solve the rolling kinematics of the honeycomb lattice. In Section 3, we solve a special case for the dynamics of this state. In Section 4, we turn to disordered lattices in $D = 2$, using a Fokker-Planck approach to show the basis for the anti-ferromagnetic ordering and the analogy to spin glasses. We also comment on the applicability of these results to the three-dimensional case. In Section 5, we conclude.

2   Kinematics of Rolling States

Consider a set of N_g spherical grains of diameter d, indexed by i, in D dimensions with velocities $\vec{v}_i$ and rotational velocities (in $D = 2$ or $D = 3$, the generalization to higher dimensions is obvious) $\vec{\omega}_i$. We further suppose the existence of pairs of grains $\langle ij \rangle$ in contact with one another, and for which there is no relative motion of

the surface points in contact (corresponding to frictional locking of the particles.) Suppose that the vector connecting the pair $\langle ij \rangle$ is $\delta \vec{w}_{\langle ij \rangle}$, with $|\delta \vec{w}_{\langle ij \rangle}| = d$. Then the requirement that the relative motion of the surface points in contact be zero is

$$\vec{v}_i - \vec{v}_j \equiv \delta \vec{v}_{\langle ij \rangle} = \frac{1}{2}(\vec{\omega}_i + \vec{\omega}_j) \times \delta \vec{w}_{\langle ij \rangle}. \tag{8}$$

Taking the derivative with respect to time of this constraint yields a constraint for the accelerations of the grains $\vec{a}_i$ and angular accelerations $\vec{\Gamma}_i$

$$\delta \vec{a}_{\langle ij \rangle} = \frac{1}{2}(\vec{\omega}_i + \vec{\omega}_j) \times \delta \vec{v}_{\langle ij \rangle} + \frac{1}{2}(\vec{\Gamma}_i + \vec{\Gamma}_j) \times \delta \vec{w}_{\langle ij \rangle}. \tag{9}$$

These equations substantially constrain both the motion of the grains and the forces between the grains. Equation (8) gives $D - 1$ constraints per contact. The requirement that the grains stay in contact gives one further constraint. Since each particle has $D(D + 1)/2$ degrees of freedom without contacts, this means that the total number of degrees of freedom N_F is

$$\frac{N_F}{N_g} = \frac{D}{2}(D + 1 - Z_c), \tag{10}$$

where Z_c is the average coordination number of the grains. We thus see that the average coordination $Z_c \leq D + 1$ in order for the rolling state to be mobile at all, and Eq. (10) then gives the effective number of degrees of freedom remaining to the packing.

Note that the coordination number can exceed this value if some of the contacts are sliding instead of rolling. In this case, there are D constraints per rolling contact, and only one constraint at a sliding contact. If we write the average number of rolling and sliding contacts per particle respectively as Z_C^R and Z_C^S, then[16]

$$\frac{N_F}{N_g} = \left[\frac{D}{2}(D + 1) - \frac{D}{2} Z_c^R - \frac{1}{2} Z_C^S \right], \tag{11}$$

which is similar to an "isostatic" argument for a packing with a mixture of Coulomb saturated and unsaturated contacts [17].

The forces are even more completely determined. The total number of contact forces is exactly the same as the number of constraints on the accelerations given by Eq. (9), with the result that all of these forces are determined by the contact network, the velocities and angular velocities of the particles, and the boundary conditions, even for $Z_c < D + 1$. (This result can be extended to the case of sliding contacts [18].)

With the kinematics thus determined, the equations of motion of the particles can be integrated until one of two possible types of crisis occurs to disrupt the network (See Figure 1).

1. If two grains collide, they will very rapidly (within a collision time set by the Young's modulus of the particles) establish a contact with a finite normal force, provided they are sufficiently inelastic. This also changes the network, and hence the kinematics. In this case the impulse arising from the collision will, in general, result in a jump in the velocities and forces, which may be significant in the neighborhood of the new contact. Corresponding to the change in kinetic
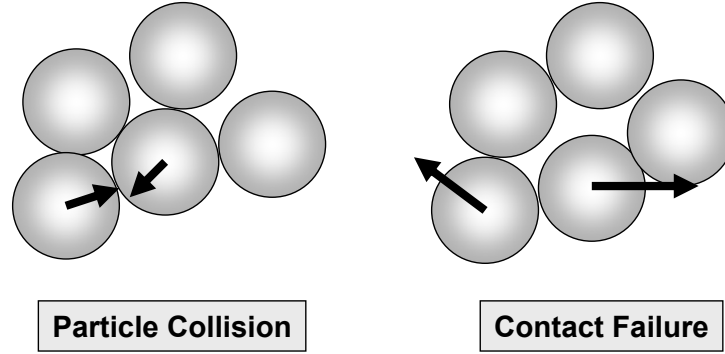
Figure 1: Two types of crisis can disrupt a lattice of rolling grains: a) two grains collide, creating a new contact, or b) two grains separate due to the normal force between them reaching zero.

energy caused by the velocity jumps there will be a net energy dissipation corresponding to the collision event [19].

2. If the normal force between two grains becomes zero, the grains will separate. This effectively changes the contact network, and the kinematics must now be solved with the new contact network. However, we do not anticipate that this change in kinematics will correspond to any jump in the velocities or forces. This event does not lead to any dissipation.

In a statistical steady state, the number of contact failures per unit time should equal the number of new contacts created by collisions per unit time.

2.1   The Honeycomb Lattice

In $D = 2$, we can construct an explicit example of a rolling state at the critical coordination number $Z_c = 3$ by considering a honeycomb lattice (Figure 2). We consider a relatively symmetric lattice, characterized by one angle θ; the basic plaquettes of the lattice are equilateral (although not necessarily regular) hexagons.

We describe the system as a lattice of "doublets" made up of two grains in contact. The positions of these doublets we index by (j, k), with either j, k both even, or j, k both odd. The positions of the centers of the doublets are then $(x, y) = (c_x j, c_y k)$, with $c_x = d(1 + \cos\theta)$ and $c_y = d\sin\theta$. Note that the axes of the Bravais lattice of doublets are oriented along the angles $\pm\theta/2$. With the doublets oriented along the x-axis, the requirement that the two grains stay in contact and have a rolling contact constrains the velocities and rotational velocities of the left-hand and right-hand grains, $u_x^L, u_y^L, \Omega^L; u_x^R, u_y^R, \Omega^R$

$$u_x^L = u_x^R \equiv u_x, \quad u_y^L \equiv u_y - \tfrac{d}{4}(\Omega^L + \Omega^R), \quad u_y^R \equiv u_y + \tfrac{d}{4}(\Omega^L + \Omega^R) \ , \qquad (12)$$

which reduces the six degrees of freedom of the two grains taken independently to the four degrees of freedom remaining after the imposition of the constraint that the contact be a permanent, rolling contact. These four degrees of freedom are conveniently taken as the average x and y velocities of the doublet, u_x, u_y, and two
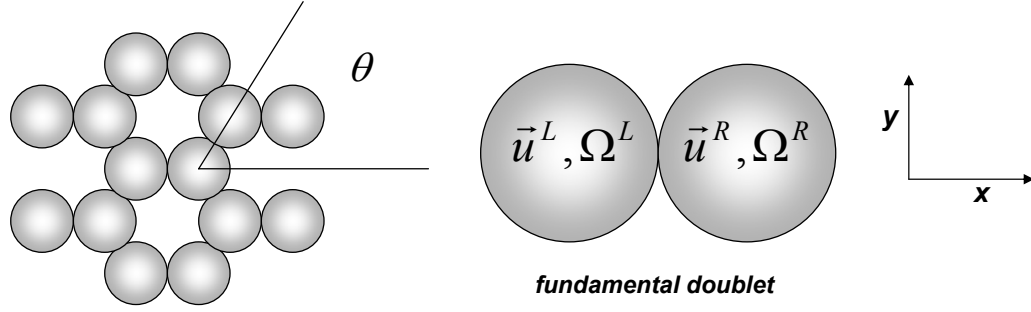
Figure 2: A honeycomb lattice has the critical coordination number $Z_c = 3$ at which a frictional packing becomes mobile in $D = 2$. We work with a set of honeycomb lattices characterized by the single parameter θ. We also show the fundamental "doublet" and the coordinate system.

(re-dimensioned) combinations of the two rotational velocities $\Delta = \frac{d}{2}(\Omega^L + \Omega^R)$, $\xi = \frac{d}{2}(\Omega^L - \Omega^R)$.

Now let us consider the constraints imposed by the requirement that the contacts between the doublet and other grains be rolling. Consider the contacts between the doublet at j, k and the doublets at $j - 1, k - 1$ and $j + 1, k - 1$. Let us write the vector $z(j, k)$ describing the doublet kinematical state,

$$z(j, k) = (u_x(j, k), u_y(j, k), \Delta(j, k), \xi(j, k)). \tag{13}$$

The contact rolling equations have the form

$$z(j, k) = \bar{A}_- z(j - 1, k - 1) + \bar{A}_+ z(j + 1, k - 1), \tag{14}$$

with $\bar{A}_-(\theta)$ and $\bar{A}_+(\theta)$ given, after some labor, by

$$\bar{A}_- = \begin{pmatrix} \frac{1}{2} & \frac{1}{2}\tan(\frac{\theta}{2}) & 0 & \frac{1}{4}\tan(\frac{\theta}{2}) \\ \frac{\cot(\theta)}{2} & \frac{1}{2} & \frac{1}{4} & 0 \\ 0 & -\frac{1}{1+\cos\theta} & -\frac{1}{2} & \frac{1}{2}\frac{\cos\theta}{1+\cos\theta} \\ \csc\theta & 0 & -\frac{1}{2} & \frac{1}{2} \end{pmatrix}, \tag{15}$$

and

$$\bar{A}_+ = \begin{pmatrix} \frac{1}{2} & -\frac{1}{2}\tan(\frac{\theta}{2}) & 0 & -\frac{1}{4}\tan(\frac{\theta}{2}) \\ -\frac{\cot(\theta)}{2} & \frac{1}{2} & -\frac{1}{4} & 0 \\ 0 & \frac{1}{1+\cos\theta} & -\frac{1}{2} & -\frac{1}{2}\frac{\cos\theta}{1+\cos\theta} \\ -\csc\theta & 0 & \frac{1}{2} & \frac{1}{2} \end{pmatrix}. \tag{16}$$

Solutions to Eq. (14) can be written in the Bloch-Floquet form

$$z(j, k) = \int_{-\pi/2}^{\pi/2} \frac{dq}{\pi} e^{\iota q j} \sum_{n=1}^{4} \alpha_n(q)(\lambda_n(q))^k v_n(q), \tag{17}$$

with

$$\bar{A}(q)v_n(q) = \lambda_n(q)v_n(q), \tag{18}$$

where $\bar{A}(q)$ is

$$\bar{A}(q) = \cos(q)\begin{pmatrix} 1 & 0 & 0 & 0 \\ 0 & 1 & 0 & 0 \\ 0 & 0 & -1 & 0 \\ 0 & 0 & 0 & 1 \end{pmatrix} + \imath\sin(q)\begin{pmatrix} 0 & -\tan(\frac{\theta}{2}) & 0 & -\frac{1}{2}\tan(\frac{\theta}{2}) \\ -\cot(\theta) & 0 & -\frac{1}{2} & 0 \\ 0 & \frac{2}{1+\cos\theta} & -1 & -\frac{\cos\theta}{1+\cos\theta} \\ -2\csc\theta & 0 & 1 & 0 \end{pmatrix}.$$

$$(19)$$

We can now directly diagonalize $\bar{A}(q)$ to obtain the eigenvalues and eigenvectors.

$$\{\lambda_1(q); v_1\} = \{-1; [0, -1/2, \imath\cot(q/2), 1]\}, \tag{20}$$

$$\{\lambda_2(q); v_2\} = \{1; [0, -1/2, -\imath\tan(q/2), 1]\}, \tag{21}$$

$$\{\lambda_3(q); v_3\} = \{e^{-\imath q}; [\frac{\sin\theta}{2}, \frac{\cos\theta}{2}, 0, 1]\}, \tag{22}$$

$$\{\lambda_4(q); v_4\} = \{e^{\imath q}; [-\frac{\sin\theta}{2}, \frac{\cos\theta}{2}, 0, 1]\}. \tag{23}$$

These modes can obviously be combined to give a wide variety of different possible motions. We are most interested, however, in motions corresponding to low wavenumber deformations of the lattice. With some manipulations, we can determine the general solution for constant velocity gradients. With $\beta_{1,2,3,4} \in \Re$, we write

$$z(j, k) = \begin{pmatrix} \frac{\sin\theta}{2}(\beta_3(j-k) - \beta_4(j+k)) \\ \frac{\cos\theta}{2}(\beta_3(j-k) + \beta_4(j+k)) - \frac{\beta_2}{2}j + \frac{\beta_1}{4}(-1)^k \\ \beta_1 j(-1)^k \\ \beta_2 j + \beta_3(j-k) + \beta_4(j+k) - \frac{\beta_1}{2}(-1)^k \end{pmatrix}. \tag{24}$$

Note that for $\beta_1 \neq 0$, but $\beta_{2,3,4} = 0$, there is no large-scale motion of the lattice, but rather compensating motions of neighboring doublets. Although we have not introduced the concept of an excitation energy, the β_1 mode is reminiscent of "optical" modes in standard lattice dynamics, which have finite energy even at zero wave-vector, and corresponds similarly to compensating motions inside a Bravais lattice cell.

The other three modes correspond to simple shear motions. The β_2 mode corresponding to shear along the y-direction (Figure 3), while the β_3 and β_4 modes corresponding to flow perpendicular to the directions $\pm\theta$. (see Figure 4). Flows such as extensional flows that combine simple shear motions can be easily constructed from these three simple shearing modes.

It is notable that in all of the simple shearing modes, the parameter $\xi = \frac{d}{2}(\Omega^L - \Omega^R)$ increases linearly across the shearing region (Figure 3). While the average angular velocity $\langle\omega\rangle$ obeys

$$\langle\omega\rangle \sim \dot{\gamma}, \tag{25}$$

where $\dot{\gamma}$ is the overall shear, the average value of the angular velocity squared, $\langle\omega^2\rangle$ depends additionally on the size of the system (or of the coherently shearing region within the system) ℓ,

$$\langle\omega^2\rangle \sim \left(\frac{\dot{\gamma}\ell}{d}\right)^2. \tag{26}$$
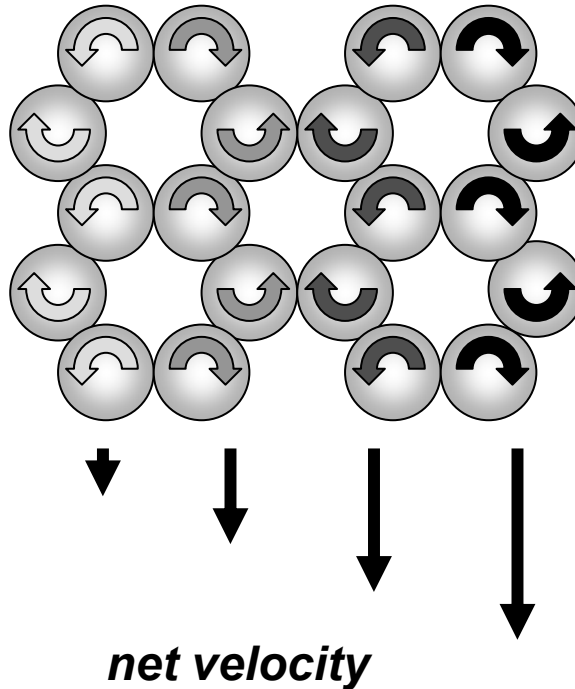
Figure 3: The β_2 mode from Eq. (24) corresponds to grains counter-rotating in each vertical chain, with the magnitude of the rotations increasing linearly with the coordinate x. This generates an overall pure shear, with the velocity in the vertical direction.

3   Forces in Rolling States

Simply showing that a state is kinematically possible does not imply that it is dynamically feasible–to accomplish this latter, we must also determine a set of interparticle forces with which it is consistent. For a granular system, this will be a set of normal forces N and tangential forces T across each contact, subject to the two constraints that $N > 0$, since grains cannot exert tensional forces on one another, and $T \leq \mu N$, with μ the coefficient of friction.

Note that despite the fact that we are considering rolling contacts, we assume that any value of $T \leq \mu N$ is admissible, and do not restrict ourselves to values of T corresponding to "free rolling" [19]. This is due to the fact that our particles are in general constrained by several contact forces, so the contact dynamics will be governed by the laws of "tractive rolling", which allow any value of $T \leq \mu N$.

Returning to our honeycomb lattice, consider a doublet at position (j, k). Such a doublet is influenced by 8 forces exerted across its 4 contacts, as well as by two internal forces exerted by the two grains on one another. It is convenient to use a geographical notation to describe the external forces– the forces exerted by the doublet at $(j - 1, k + 1)$ on the doublet at (j, k) are termed N_{NW}, T_{NW}, with T defined so that a force in the counter-clockwise direction is positive. Similarly, we define the forces exerted by the $(j + 1, k + 1)$, $(j + 1, k - 1)$ and $(j - 1, k - 1)$ doublets respectively as (N_{NE}, T_{NE}), (N_{SE}, T_{SE}), and (N_{SW}, T_{SW}) (see Figure 5).
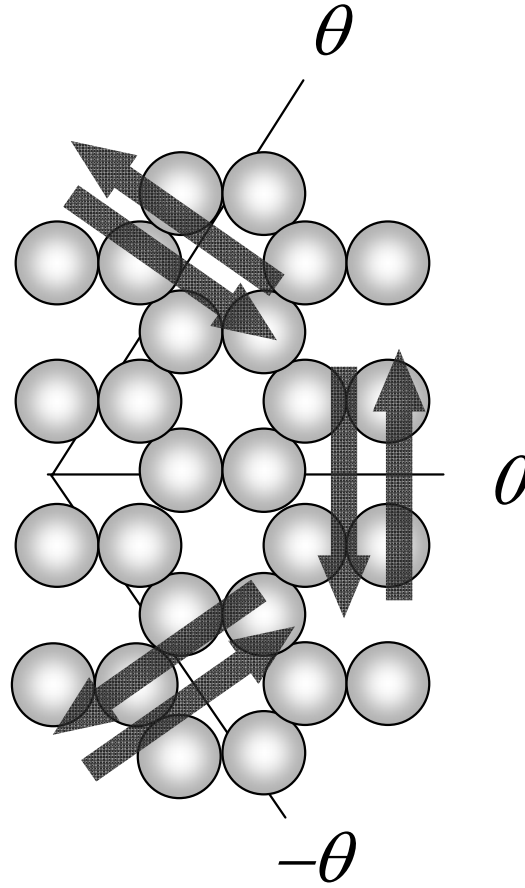
Figure 4: The three acoustic modes of the kinematics correspond to shear directed perpendicular to the y-axis, and perpendicular to the directions $\pm\theta/2$.

The force exerted at the internal contact is (N_0, T_0), with T_0 defined so that $T_0 > 0$ corresponds to a counter-clockwise force on each grain.

With some tedious but straightforward algebra, we can convert the six equations of motion of the two particles in the doublet into four equations coupled to our natural kinematical variables, plus two equations determining the internal forces N_0, T_0 (which we here omit). We write M and I_M for the masses and moments of inertia of the grains, with $\kappa = I_M/Md^2$. The result for the dynamical equation for the doublet is [15]

$$
\begin{pmatrix} N_{NW} \\ T_{NW} \\ N_{NE} \\ T_{NE} \end{pmatrix} = \bar{B}(\theta) \begin{pmatrix} N_{SW} \\ T_{SW} \\ N_{SE} \\ T_{SE} \end{pmatrix} + 2M\bar{C}(\theta) \begin{pmatrix} \dot{u}_x \\ \dot{u}_y \\ (1+\kappa)\dot{\Delta} \\ \kappa\dot{\xi} \end{pmatrix}, \tag{27}
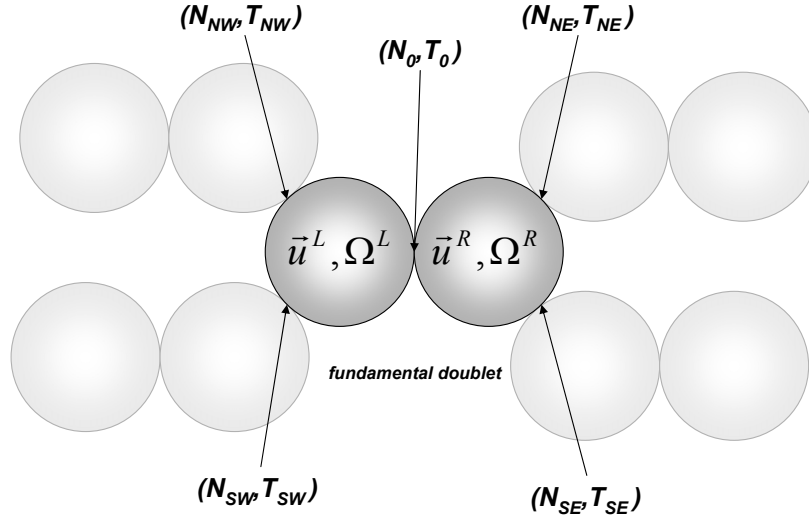$$

Figure 5: Eight forces are exerted on a fundamental doublet of the honeycomb lattice by its neighbors; two additional forces are exerted by the doublet particles on one another.

with $\bar{B}(\theta)$ and $\bar{C}(\theta)$ given by

$$\bar{B}(\theta) = \begin{pmatrix} 2\sin^2(\theta/2) & -\sin\theta & \cos\theta & -\sin\theta \\ \sin\theta - \tan(\theta/2) & -\cos\theta & -\sin\theta + \tan(\theta/2) & 2\sin^2(\theta/2) \\ \cos\theta & \sin\theta & 2\sin^2(\theta/2) & \sin\theta \\ \sin\theta - \tan(\theta/2) & 2\sin^2(\theta/2) & -\sin\theta + \tan(\theta/2) & -\cos\theta \end{pmatrix}, \quad (28)$$

and

$$\bar{C}(\theta) = \frac{1}{2} \begin{pmatrix} 1 & -\csc\theta & \tan(\theta/2) & -\cot\theta \\ -\tan(\theta/2) & 0 & \frac{\cos\theta}{1+\cos\theta} & 1 \\ -1 & -\csc\theta & -\tan(\theta/2) & -\cot\theta \\ -\tan(\theta/2) & 0 & \frac{\cos\theta}{1+\cos\theta} & -1 \end{pmatrix}, \quad (29)$$

Note that $(N_{SW}(j,k), T_{SW}(j,k)) = (N_{NE}(j-1,k-1), T_{NE}(j-1,k-1))$, with equivalent identities for the other forces. The forces can be written as

$$\begin{pmatrix} N_{NW}(j,k) \\ T_{NW}(j,k) \\ N_{NE}(j,k) \\ T_{NE}(j,k) \end{pmatrix} = \int_{-\pi/2}^{\pi/2} \frac{dq}{\pi} e^{iqj} \begin{pmatrix} N_{NW}(q,k) \\ T_{NW}(q,k) \\ N_{NE}(q,k) \\ T_{NE}(q,k) \end{pmatrix}. \quad (30)$$

We then can immediately write the equation determining solutions to the homogeneous problem,

$$\begin{pmatrix} N_{NW}(q,k) \\ T_{NW}(q,k) \\ N_{NE}(q,k) \\ T_{NE}(q,k) \end{pmatrix} = \bar{B}(\theta)\bar{D}(q) \begin{pmatrix} N_{NW}(q,k-1) \\ T_{NW}(q,k-1) \\ N_{NE}(q,k-1) \\ T_{NE}(q,k-1) \end{pmatrix}, \quad (31)$$

with

$$\bar{D}(q) = \begin{pmatrix} 0 & 0 & e^{-\imath q} & 0 \\ 0 & 0 & 0 & e^{-\imath q} \\ e^{\imath q} & 0 & 0 & 0 \\ 0 & e^{\imath q} & 0 & 0 \end{pmatrix}. \tag{32}$$

The eigenvalues and eigenvectors $\{\nu_n; u_n\}$ of $\bar{\mathcal{B}}(\theta, q) = \bar{B}(\theta)\bar{D}(q)$ are given by

$$
\begin{array}{rcl}
\{\nu_1(q); u_1\} & = & \{-1; [e^{-\imath q}\tan\theta, e^{-\imath q}, -\tan\theta, 1]\}, \tag{33} \\
\{\nu_2(q); u_2\} & = & \{1; [-e^{-\imath q}\tan\theta, -e^{-\imath q}, -\tan\theta, 1]\}, \tag{34} \\
\{\nu_3(q); u_3\} & = & \{e^{-\imath q}; [0, 0, \cot(\theta/2), 1]\}, \tag{35} \\
\{\nu_4(q); u_4\} & = & \{e^{\imath q}; [-\cot(\theta/2), 1, 0, 0]\}. \tag{36}
\end{array}
$$

These eigenvectors are in fact quite intuitive. Each of the eigenvectors 2-4 corresponds to a set of parallel force chains in one direction in the lattice, as is illustrated in Figure 6; eigenvector 1 is more complex.
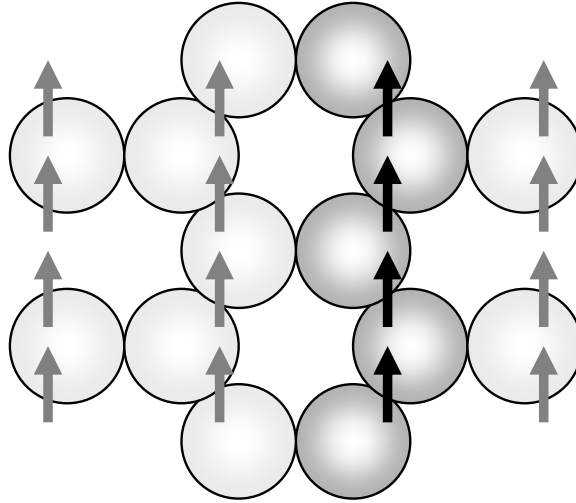

Figure 6: The fundamental homogeneous modes of the forces correspond principally to force chains, including both normal and tangential forces, directed along the lattice directions of the honeycomb lattice. The force chains shown correspond to the second force eigenvector, given in Eq. (34).

Given the homogeneous solutions, it is straightforward to determine the solution to the inhomogeneous problem for which the packing is moving. Writing

$$2M\bar{C}(\theta) \begin{pmatrix} \dot{u}_x(q, k) \\ \dot{u}_y(q, k) \\ (1+\kappa)\dot{\Delta}(q, k) \\ \kappa\dot{\xi}(q, k) \end{pmatrix} = \sum_{n=1}^{4} v_n(q, k) u_n(\theta, q), \tag{37}$$

with

$$v_n(j, k) = \int_{-\pi/2}^{\pi/2} \frac{dq}{\pi} e^{\imath q j} v_n(q, k), \tag{38}$$

we have the inhomogeneous equation

$$
\begin{pmatrix} N_{NW}(q,k) \\ T_{NW}(q,k) \\ N_{NE}(q,k) \\ T_{NE}(q,k) \end{pmatrix} = \bar{\mathcal{B}}(\theta,q) \begin{pmatrix} N_{NW}(q,k-1) \\ T_{NW}(q,k-1) \\ N_{NE}(q,k-1) \\ T_{NE}(q,k-1) \end{pmatrix} + \sum_{n=1}^{4} \upsilon_n(q,k)u_n. \tag{39}
$$

This equation is easy to solve. Writing

$$
\begin{pmatrix} N_{NW}(q,0) \\ T_{NW}(q,0) \\ N_{NE}(q,0) \\ T_{NE}(q,0) \end{pmatrix} = \sum_{n=1}^{4} \tau_n(q)u_n, \tag{40}
$$

we immediately obtain

$$
\begin{pmatrix} N_{NW}(q,k) \\ T_{NW}(q,k) \\ N_{NE}(q,k) \\ T_{NE}(q,k) \end{pmatrix} = \sum_{n=1}^{4} \left[\sum_{k'=0}^{k-1} \nu_n^{k'} \upsilon_n(q,k-k') + \nu_n^{k}\tau_n(q) \right] u_n. \tag{41}
$$

As an example, let us consider extensional flow: $u_x \propto x$, $u_y \propto -y$. This type of flow has the advantage that it preserves the overall symmetries of the honeycomb lattice, and can thus be interpreted parametrically by making the angle θ a function of time, $\theta(t)$. Let us choose the simple case that

$$
\theta(t) = -\Lambda t + \theta_0. \tag{42}
$$

with $\Lambda > 0$.

With some labor, it is possible to determine the inhomogeneous contribution to the forces corresponding to this motion,

$$
\begin{pmatrix} N_{NW}(j,k) \\ T_{NW}(j,k) \\ N_{NE}(j,k) \\ T_{NE}(j,k) \end{pmatrix}_{inhom.}
$$

$$
= \frac{dM\Lambda^2}{2}[\cos\theta \tan(\theta/2)] \left\{ \frac{k^2}{2} \begin{pmatrix} \tan\theta \\ 1 \\ \tan\theta \\ -1 \end{pmatrix} + jk \begin{pmatrix} -\cot(\theta/2) \\ 1 \\ \cot(\theta/2) \\ 1 \end{pmatrix} \right\}. \tag{43}
$$

where we have neglected terms of less than quadratic order in j,k.

It is clear that this inhomogeneous contribution includes negative values of the normal forces at sufficiently low values of k/j, and that these scale with k^2 (at fixed k/j). In addition, it is also easy to determine the inhomogeneous part of the internal normal force within a doublet, $N_{0,inhom.}$ (at quadratic order in j,k) [15],

$$
N_{0,inhom.} = -\frac{dM\Lambda^2 \sin\theta}{2}k^2 \tag{44}
$$

which is also negative, and also scales with k^2.

Thus, no matter what the value of the homogeneous term for the forces (corresponding to the term proportional to τ in Eq. (41)), the requirement that normal forces be positive will ultimately be overwhelmed by the growth of the inhomogeneous term. Note that it is the contacts most perpendicular to the direction of acceleration that are most at risk of losing their normal forces. In addition, with a finite coefficient of friction, the tangential forces will ultimately saturate the Coulomb criterion and slippage will occur at grain contacts, invalidating our kinematical assumptions. However, even with an *infinite* coefficient of friction, the motion of the packing is limited to a domain size controlled by the requirement that all normal forces be compressional. If the scale of the homogeneous forces is determined by the average pressure in the packing P, then the scale ℓ of this domain size is determined by

$$\frac{\ell}{d} = \frac{1}{\Lambda d}\sqrt{P/\rho_g},\tag{45}$$

with the density $\rho_g \sim M/d^2$. Comparing to Eqs. (3), we see that this is equivalent to

$$\ell = \frac{d}{I},\tag{46}$$

which connects the length scale over which frictionally dominated motion can determine the kinematics with the Inertia Number I, in a manner consistent with the physical picture of Halsey and Ertaş.

Note that this result can also be obtained on dimensional grounds. The accelerations in a shearing state, as determined in the above calculation, will typically be directed normal to the contacts, leading to a local relative acceleration of

$$\vec{a}_i - \vec{a}_j \sim \dot{\gamma}^2 d.\tag{47}$$

However, if the motions are coherent, as in a shearing motion, then accelerations will accumulate across a region ℓ, so that the typical acceleration in this region will be

$$\vec{a}_i \sim \dot{\gamma}^2 \ell.\tag{48}$$

Similarly, the forces will need to accumulate to drive these accelerations, so we conclude that the force scale will be

$$N \sim M\frac{(\dot{\gamma}\ell)^2}{d}\tag{49}$$

which is the scale of the inhomogeneous forces computed explicitly above. This follows entirely from the coherent nature of the accelerations, and does not require that the contacts be rolling. Thus, any state in which Eqs. (47,48,49) hold will also have its regions of coherent shear limited to the scale $\ell = d/I$, including much more disorderly states than the honeycomb lattice. I will return to this point in Section 4 below.

4   Kinematics of Random Grain Packings

Let us reconsider the kinematics of the honeycomb lattice state, as defined by
Eq. (17). An initially surprising feature of this state is the role played by $\xi = \frac{d}{2}(\Omega^L - \Omega^R)$, which increases linearly with distance in states with overall linear be-
havior of the average velocities u_x and u_y. Thus, one way to view the motion of the
honeycomb state is by decomposing it into alternating sub-lattices, A and B (see
Figure 7), on which the particles are approximately counter-rotating with respect
to one another. The spatial variations of these counter-rotations then determine the
overall spatial structure of the flow. Now we must consider random lattices, and
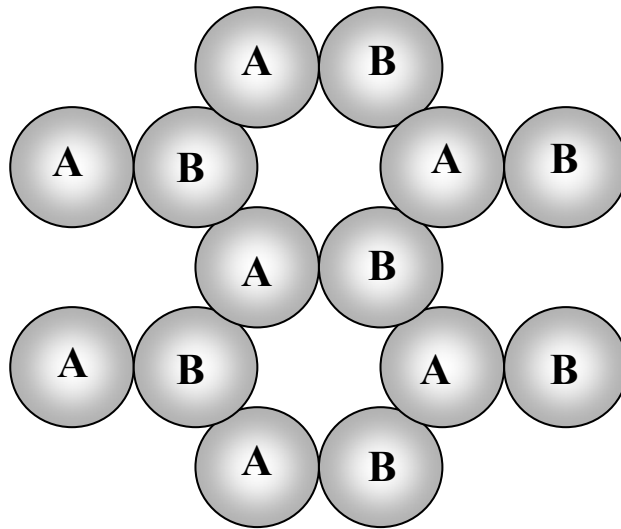determine, in particular, if there is any remnant of this feature for such lattices.

Figure 7: The honeycomb lattice shear solutions correspond to approximate counter-rotation of
two alternating sublattices of grains, here indexed by A,B.

To determine the nature of the random lattice solution that respects the
constraining large-scale motions, we apply a two-point Fokker-Planck approxima-
tion. Consider a random walk that moves entirely between grains in contact with
one another (see Figure 8). Provided that the instantaneous contact network per-
colates, such a random walk can access arbitrarily distantly separated parts of the
grain packing. Over the set of all particle contacts $\langle ij \rangle$ we can define a probability
distribution $\rho(\theta, \delta\vec{v})$ on the angles of the contacts θ_{ij} and the differences in grain
velocity across the contacts $\delta\vec{v}_{ij} = \vec{v}_i - \vec{v}_j$. For simplicity of notation we are confining
ourselves to two dimensions; however, the generalization to arbitrary dimensions is
clear, and is assumed in much of the discussion below.

We now assume that in the random walk described in the previous paragraph,
subsequent steps in the random walk correspond to uncorrelated choices of $\theta_{ij}, \delta\vec{v}_{ij}$
from the distribution $\rho(\theta, \delta\vec{v})$. (The neglect of correlations in this approximation is
clearly dangerous, particularly in lower dimensionalities, of which more later.)

Let us define a matrix corresponding to the average changes in position and
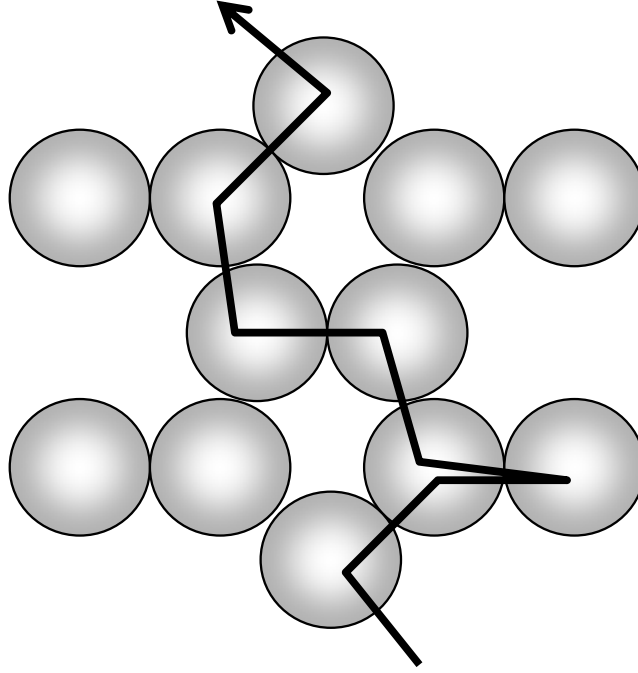velocity corresponding to one step in this random walk,

Figure 8: In the Fokker-Planck approximation, we consider random walks from grain to grain passing always through contacts between the grains.

$$\bar{\mathcal{M}} = \left(\begin{array}{cccc} \langle \delta w_x \delta w_x \rangle & \langle \delta w_x \delta w_y \rangle & \langle \delta w_x \delta v_x \rangle & \langle \delta w_x \delta v_y \rangle \\ \langle \delta w_y \delta w_x \rangle & \langle \delta w_y \delta w_y \rangle & \langle \delta w_y \delta v_x \rangle & \langle \delta w_y \delta v_y \rangle \\ \langle \delta v_x \delta w_x \rangle & \langle \delta v_x \delta w_y \rangle & \langle \delta v_x \delta v_x \rangle & \langle \delta v_x \delta v_y \rangle \\ \langle \delta v_y \delta w_x \rangle & \langle \delta v_y \delta w_y \rangle & \langle \delta v_y \delta v_x \rangle & \langle \delta v_y \delta v_y \rangle \end{array} \right). \tag{50}$$

In this matrix, the averages are easily written, e.g.

$$\langle \delta w_x \delta w_x \rangle = \int d\theta \int d(\delta \vec{v}) \rho(\theta, \delta \vec{v})(d \cos \theta)^2. \tag{51}$$

We can now write directly the limiting result for the probability distribution $\rho_n(\Delta \vec{w}, \Delta \vec{v})$ after n steps of the random walk, with $n \to \infty$,

$$\rho_n(\Delta \vec{w}, \Delta \vec{v}) = \frac{1}{\sqrt{(2\pi n)^4 \det(\bar{\mathcal{M}})}} \exp \left\{ -\frac{1}{2n} \left[\left(\Delta \vec{w} \quad \Delta \vec{v} \right) \bar{\mathcal{M}}^{-1} \left(\begin{array}{c} \Delta \vec{w} \\ \Delta \vec{v} \end{array} \right) \right] \right\}. \tag{52}$$

We can use this probability distribution to compute properties of the velocity distribution arising from the fundamental two-particle correlations expressed in $\bar{\mathcal{M}}$. Thus the expectation value of the velocity at the spatial point $\vec{x}$ is given by

$$\langle \vec{v}(\vec{x}) \rangle = \frac{\int dn \int d\vec{v}(\vec{v}) \rho_n(\vec{x}, \vec{v})}{\int dn \int d\vec{v} \rho_n(\vec{x}, \vec{v})}. \tag{53}$$

As an example, consider a case in which $\langle \delta w_x \delta w_y \rangle = \langle \delta v_x \delta v_y \rangle = 0$, and $\langle \delta w_x \delta v_x \rangle = \langle \delta w_y \delta v_y \rangle = \langle \delta w_y \delta v_x \rangle = 0$, but in which $\langle \delta w_x \delta v_y \rangle \neq 0$. In this case we can write

$$\bar{\mathcal{M}} = \begin{pmatrix} \langle \delta w_x \delta w_x \rangle & 0 & 0 & \langle \delta w_x \delta v_y \rangle \\ 0 & \langle \delta w_y \delta w_y \rangle & 0 & 0 \\ 0 & 0 & \langle \delta v_x \delta v_x \rangle & 0 \\ \langle \delta v_y \delta w_x \rangle & 0 & 0 & \langle \delta v_y \delta v_y \rangle \end{pmatrix}. \tag{54}$$

We can now invert $\mathcal{M}$ and use Eq. (53) to show that

$$\frac{\partial \langle v_y \rangle}{\partial x} = \frac{\langle \delta w_x \delta v_y \rangle}{\langle (\delta w_x)^2 \rangle}, \tag{55}$$

and

$$\frac{\partial \langle v_x \rangle}{\partial x} = \frac{\partial \langle v_{x,y} \rangle}{\partial y} = 0, \tag{56}$$

corresponding to pure shear motion.

In this way, any motion that is linear in the coordinates can be associated with values of the coefficients of the matrix $\bar{\mathcal{M}}$, corresponding to particular correlations of neighboring grains. This approach has an interesting feature; however, in that it leads to divergent fluctuations in dimensions below $D = 4$.

The generalization of the above formulae to $\rho_n^{(D)}(\vec{x}, \vec{v})$ with $D > 2$ is simple, so we can consider, for instance,

$$\langle (\vec{v}(\vec{x}) - \langle \vec{v}(\vec{x}) \rangle)^2 \rangle = \lim_{N \to \infty} \frac{\int_0^N dn \int d\vec{v}(\vec{v}^2 - \langle \vec{v} \rangle^2) \rho_n^{(D)}(\vec{x}, \vec{v})}{\int_0^N dn \int d\vec{v} \rho_n^{(D)}(\vec{x}, \vec{v})}. \tag{57}$$

Simple power-counting leads immediately to the conclusion that

$$\langle (\vec{v}(\vec{x}) - \langle \vec{v}(\vec{x}) \rangle)^2 \rangle \sim N^{2-D/2}. \tag{58}$$

If we suppose that $\ell \sim \sqrt{N}$ corresponds to some maximum "coherent" length scale that can be probed by the random walk, then we see that

$$\langle (\vec{v}(\vec{x}) - \langle \vec{v}(\vec{x}) \rangle)^2 \rangle \sim \ell^{4-D}. \tag{59}$$

Note that assuming that $I = d/\ell$, as is done in the theory of incline flow of Halsey and Ertaş [4], gives a divergence of the squared velocity fluctuation

$$\langle (\vec{v}(\vec{x}) - \langle \vec{v}(\vec{x}) \rangle)^2 \rangle \sim I^{D-4}, \tag{60}$$

compared to the numerical result

$$\langle (\vec{v}(\vec{x}) - \langle \vec{v}(\vec{x}) \rangle)^2 \rangle \sim I^{-\chi}. \tag{61}$$

The numerical results for the values of χ in $D = 2, 3$ are not definitive on its actual value, although $\chi \approx 1$ in $D = 2$ is likely [6], and a similar and perhaps smaller value seems to hold in $D = 3$ [7].

It is striking that an argument with so little physics predicts a divergence of the velocity fluctuations, and with an exponent similar to that observed numerically [6, 7]. However, the neglect of correlations undermines the quantitative credibility of this argument[1].

---

[1]Note that a similar argument could be used for a molecular fluid, in which case it would clearly be wrong, by equipartition– highlighting the importance of correlations.

Up to now, we have not implemented any requirement that the velocities be determined by the angular motions of the particles. This is seemingly quite straightforward, e.g. the averages of $\delta\vec{v}$ appearing in $\bar{\mathcal{M}}$ can easily be written in terms of the angular motions of the particles, using Eq. (8), for the rolling contacts. Then, as remarked above, the percolation of the contact network insures that we can still construct the master probability distribution for the fluctuations of $\Delta\vec{w}, \Delta\vec{v}$, as in the above argument. There is, however, a subtle and important flaw in this procedure.

Restricting ourselves for the moment to two dimensions, let us try to determine large scale variations in the angular velocities Ω_i using a procedure analogous to that we used above for large scale variations in the velocity. Since the velocity moments for neighboring particles are functions of the sum of the angular velocities, $\vec{v}_i - \vec{v}_j = \hat{z} \times (\vec{w}_i - \vec{w}_j)(\Omega_i + \Omega_j)$, we will restrict ourselves to these variables in computing large-scale variations of Ω, which is feasible provided we consider the combination of two successive steps on the lattice of rolling contacts.

If we construct an analogous formula to Eq. (52) for the evolution of the distribution of Ω over a random walk, we can write

$$\frac{\partial\Omega}{\partial x} = \frac{\langle\delta w_x\delta\Omega\rangle}{\langle(\delta w_x)^2\rangle}. \tag{62}$$

Note that we have assumed above that there is a stationary distribution $\rho(\theta, \delta\vec{v}_{ij})$. If such a distribution is not a function of position, then there is no local indicator of position arising either from the angular distribution of contacts, nor from the nearest-neighbor velocity differences. For rolling contacts, this implies, as utilized in the above, a stationary distribution $\rho(\theta, \Omega_i + \Omega_j)$. To use this to evaluate an average of $\Omega_i - \Omega_j$, we can concatenate two subsequent steps in our random walk, from $i \rightarrow j \rightarrow k$, and write that for this compound step

$$\begin{aligned} \langle\delta w_{x;i\rightarrow k}(\Omega_k - \Omega_i)\rangle = \\ \langle(\delta w_{x;i\rightarrow j} + \delta w_{j\rightarrow k}) \times [(\Omega_k + \Omega_j) - (\Omega_j + \Omega_i)]\rangle = \\ d\langle\cos\theta_{ij}(\Omega_i + \Omega_j) - \cos\theta_{jk}(\Omega_j + \Omega_k)\rangle = 0, \end{aligned} \tag{63}$$

so that we conclude that it is not possible for a distribution with a stationary $\rho(\theta_{ij}, \Omega_i + \Omega_j)$ to describe a grain packing with any large-scale spatial variation of Ω.

However, inspired by the discussion above regarding the role of $\xi = \frac{d}{2}(\Omega_A - \Omega_B)$ in the honeycomb lattice case, we can immediately construct an exception to this. Suppose the packing of grains connected by rolling contacts can be described as consisting of two disjoint sub-packings A and B, so that no two A grains, nor any two B grains, are in rolling contact with one another. In this case, we can posit that the distribution used in the random walk depends on whether one is passing from an A grain to a B grain or vice versa, i.e. $\rho_{AB}(\theta, \Omega_A + \Omega_B) \neq \rho_{BA}(\theta, \Omega_B + \Omega_A) = \rho_{AB}(\theta + \pi, \Omega_A + \Omega_B)$, where this latter requirement follows from the reversibility of the random walk. Then we see that in this case, supposing that i, k are on the A packing, and j is on the B packing,

$$\begin{aligned} \langle\delta w_{x;i\rightarrow k}(\Omega_k - \Omega_i)\rangle = \\ \langle(\delta w_{x;i\rightarrow j} + \delta w_{j\rightarrow k})[(\Omega_k + \Omega_j) - (\Omega_j + \Omega_i)]\rangle = \\ 2d\langle\cos\theta_{ij}(\Omega_i + \Omega_j)\rangle_{AB}, \end{aligned} \tag{64}$$

where $\langle\rangle_{AB}$ is defined as the integral over $\rho_{AB}(\theta, \Omega_A + \Omega_B)$. Now we can develop linear gradients in Ω on sub-lattice A, provided that the gradient of Ω on the alternating sub-lattice B has the opposite sign, as in the honeycomb lattice solution.

Thus, the state will be characterized by a function $\Omega_A(x, y)$ on the A sub-lattice, and by $\Omega_B(x, y)$ on the B sub-lattice, with

$$\frac{\partial\langle\Omega_A\rangle}{\partial x} \approx -\frac{\partial\langle\Omega_B\rangle}{\partial x} \approx \frac{\langle\cos\theta_{ij}(\Omega_i + \Omega_j)\rangle_{AB}}{d\langle(\cos\theta_{ij})^2\rangle_{AB}} \tag{65}$$

This criterion will enforce that relative local particle surface velocities will be small where an A-lattice particle contacts a B-lattice particle, which is suitable to a slowly strained system with frictional contacts. Both Ω_A and Ω_B vary linearly across a shearing region. Thus, the dimensional constraint on the forces, Eq. (49), should still apply for random lattices, resulting in a restriction of the coherently shearing region to a scale $\ell = d/I$. Finally, the overall shear is determined in this case by

$$\frac{\partial\langle v_y\rangle}{\partial w_x} = \frac{\langle\cos^2\theta_{ij}(\Omega_i + \Omega_j)\rangle_{AB}}{2d\langle(\cos\theta_{ij})^2\rangle_{AB}}. \tag{66}$$

To build an explicit example of a shearing state on a random graph, suppose that we fix the rotations on the A and B sub-lattices to be simple functions of position alone,

$$\Omega_A = \Omega_A(\vec{x}) = \Omega_A^{(0)} + \vec{\Omega}_A^{(1)} \cdot \vec{x}, \tag{67}$$

$$\Omega_B = \Omega_B(\vec{x}) = \Omega_B^{(0)} + \vec{\Omega}_B^{(1)} \cdot \vec{x}. \tag{68}$$

Then for two particles in contact at positions $\vec{x}$ and $\vec{x} + \delta\vec{w}$,

$$\Omega_A(\vec{x}) + \Omega_B(\vec{x} + \vec{w}) = (\Omega_A^{(0)} + \Omega_B^{(0)}) + (\vec{\Omega}_A^{(1)} + \vec{\Omega}_B^{(1)}) \cdot \vec{x} + \Omega_B^{(0)} \cdot \delta\vec{w}. \tag{69}$$

In order for local velocity gradients to be independent of position, as in the above, we need

$$\vec{\Omega}_B^{(1)} = -\vec{\Omega}_A^{(1)} \equiv \vec{\Gamma}, \tag{70}$$

and we also write, for convenience

$$\Omega_A^{(0)} + \Omega_B^{(0)} = \varphi. \tag{71}$$

Since we have fixed the angular velocities $\Omega_{A,B}$ as functions of position alone, we can suppress the dependence of ρ_{AB} on $\Omega_A + \Omega_B$, and approximate

$$\rho_{AB}(\theta) = \rho_0 + \rho_1\vec{b} \cdot \delta\vec{w} + O(\vec{w}^2), \tag{72}$$

with, of course,

$$\delta\vec{w} = d(\cos\theta, \sin\theta). \tag{73}$$

Reviewing Eqs. (55,66), we see that to lowest order in the anisotropy, the numerator of this expression will determine the overall shear structure. Thus let us consider the following tensor,

$$T_{lm,AB} = \langle\delta w_l\delta v_m\rangle_{AB} \approx \int (d\delta\vec{w})(\rho_0 + \rho_1\vec{b} \cdot \delta\vec{w})\delta w_l \left[\frac{1}{2}(\varphi + \vec{\Gamma} \cdot \delta\vec{w})\hat{z} \times \delta\vec{w}\right]_m, \tag{74}$$

where we have used the vector structure appropriate to $D = 2$ as well as the fundamental contact rolling Eq. (8). The integral is easily performed, yielding

$$T_{lm,AB} = \frac{d^2}{4}\rho_0\varphi\epsilon_{lm} + \frac{d^2}{16}\rho_1\left[\vec{b}\cdot\vec{\Gamma}\epsilon_{lm} - b_l(\epsilon_{mp}\Gamma_p) - \Gamma_l(\epsilon_{mp}b_p)\right].\qquad (75)$$

From this formula, it is easy to find, for any $\vec{b}$, the values of φ and $\vec{\Gamma}$ corresponding to any particular shearing motion. Note that it is necessary to have <u>both</u> a linear gradient in the angular velocities (non-zero $\vec{\Gamma}$) <u>and</u> anisotropy in the contact distribution among the two sub-lattices (non-zero $\vec{b}$) in order to generate a shearing motion. Of course, for any such motion, the value of $\vec{b}$ will be determined by the kinetics of the motion, so in practice such motions will be realized as functionals of $(\varphi, \vec{\Gamma})$.

In general, it is not possible to decompose a random lattice into two alternate sub-lattices such that no contacts are created among elements of a single sub-lattice. The situation is analogous to an anti-ferromagnet on a random graph, for which plaquettes bounded by odd numbers of particles are frustrated (see Figure 9) [22]. In order to preserve the structure of the state indicated above, with $\Omega_A \approx -\Omega_B$, we require that enough of the particle contacts are sliding so that all remaining contacts can be rolling contacts between grains on alternate sublattices. It then follows that ρ_{AB} is understood as the distribution across rolling contacts only, not including sliding contacts.
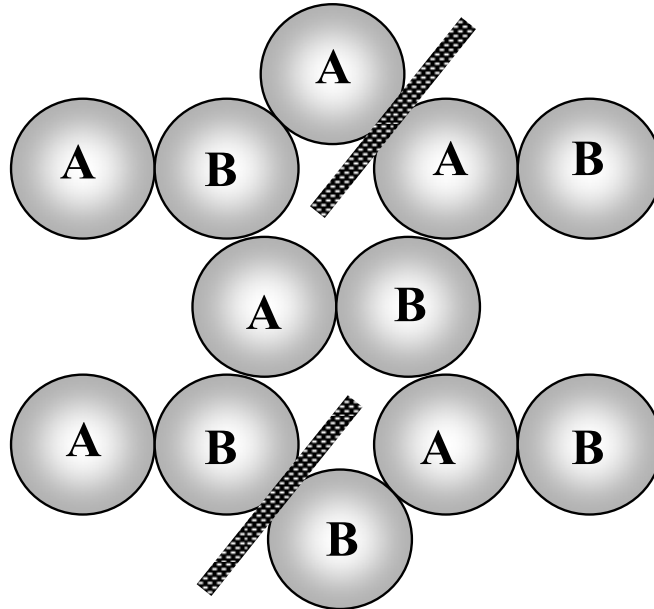

Figure 9: In a random lattice, a decomposition of the lattice into two alternating sub-lattices will generally result in "frustrated" contacts, across which sliding must occur.

If we wish to apply the reasoning of Eqs. (45-49) to the random lattice, and derive a length scale ℓ beyond which a coherently shearing patch will be destabilized by the disappearance of normal forces, we must specify what we mean by a

"coherently shearing patch" in a random lattice. For a general random lattice with some density of "odd" plaquettes, there will be a number of possible choices of which contacts must slide so that the others may roll. From the argument of the preceding paragraph, it is clear that this enumeration problem is exactly analogous to the enumeration of the states of an anti-ferromagnet on the corresponding random graph. The statistical mechanics of this latter problem has been studied–in two dimensions, there appears to be a spin-glass phase at zero temperature, which does not extend to finite temperature [21]. Although the granular problem is not a thermal statistical mechanical problem, it is natural to identify the coherence that is destroyed by the disappearing normal forces with the zero-temperature spin glass order of the analogous anti-ferromagnet. With this interpretation of the meaning of "coherence", we again expect

$$\ell = \frac{d}{I} \tag{76}$$

to set the maximum size of a coherent domain, following the argument of Eqs. (45-49). A more dramatic indicator of the existence of the state which we are discussing would be a strong short-ranged anti-ferromagnetic order corresponding to a predominance of rolling contacts.

We can contrast our results with numerical simulations reported by the group of Alonso-Marroquín et al. [20]. In a two-dimensional shear cell, this group observed that the macroscopic shearing motions of a dense granular packing (simulating fault gouge) decomposed, on smaller scales, into regions of coherent vorticity (which in our notation corresponds to Δ constant, $\xi \approx 0$), regions of "ball-bearing motion" (corresponding to the counter-rotating motion of our two sub-lattices), and shear zones in which sliding dominated. Due to the predominance of rolling contacts, particularly at high coefficients of friction, the overall macroscopic friction observed in the shear cell was considerably less than the microscopic coefficient of friction. The decomposition of the solution into regions with qualitatively different properties violates the assumption that there is a uniform distribution $\rho(\theta, \delta\vec{v})$, on which our argument above was based.

The first of the Alonso-Marroquín motions, corresponding to large-scale vorticity, was not observed in three-dimensional numerical studies specifically designed to look for velocity correlations in chute flows [7]. Also, at high coefficients of friction, the Alonso-Marroquín kinematics was "earthquake-like", with much of the slip occurring in discontinuous jumps. We might suspect that such discontinuous kinetics, associated with pattern formation, are more characteristic of low values of I (corresponding to $\ell \gg L$, with L an overall flow scale), than they are of intermediate values of I.

Finally, we are also able to use this picture to speculate on the nature of the $\mu \to \infty$ limit. Consider the tangential and normal forces T_c, N_c at a typical sliding contact, $T_c/N_c = \mu$. These forces will be determined by the overall force balances subject to the motions of the grains, and we expect that both T_c and N_c will be $\sim Pd^{D-1}$. Since these forces have a fixed ratio at the sliding contacts, we see that $\lim_{\mu \to \infty} N_c = 0$, since this will be the solution to the force balances in preference to a case in which $T_c \to \infty$. Thus, in the limit, the sliding contacts will see their normal forces driven to zero; i.e., these contacts will be eliminated as physical contacts. We would thus expect that in the limit $\mu \to \infty$ all of the plaquettes will have even numbers of sides, and the frustration will be eliminated, in any mobile state.

4.1   Three-Dimensional Case

The extension of these arguments to three dimensions is straightforward. The original contact-rolling equations Eqs. (8,9) clearly apply in three dimensions, and the diamond lattice plays the same role in $D = 3$ of a potential model system as did the honeycomb lattice in $D = 2$. To conserve the labor of the author and the patience of the reader, we are not presenting details of the diamond lattice kinematics in this work; we only wish to point out that the diamond lattice does support alternating A and B sublattices analogously to the honeycomb lattice case, which allows shearing states obeying $\vec{\Omega}_A \approx -\vec{\Omega}_B$ to be constructed.

For random lattices, the arguments of the previous section should hold in three dimensions just as in two dimensions (indeed, they should be more valid, since the upper critical dimension of $D = 4$ is closer). Again, the optimal decomposition of the random lattice into two alternating sublattices is analogous to the problem of determining a ground state for an anti-ferromagnet on a random graph. Again, odd plaquettes must have at least one sliding contact, corresponding to a frustrated bond in the random anti-ferromagnet. In three dimensions, these odd plaquettes can be viewed as threaded by "odd lines", introduced by Rivier and Duffy [23]. For pure shear, we expect the direction of the typical angular velocity to be perpendicular to the shearing motions, so that the analogy is to an Ising anti-ferromagnet, and not to a Heisenberg anti-ferromagnet. Note that the degenerate case in which particles rotate about an axis through the contact between the particles is assumed not to play a significant role.

5   Conclusions

The principal conclusions of this article are

1. Frictional packings, dominated by rolling contacts, cannot be mobile above a coordination number $Z_c = 3$ ($D = 2$) or $Z_c = 4$ ($D = 3$). These thresholds are consistent with those obtained using similar arguments by authors studying the isostaticity of static packings. These criteria are modified in a straightforward manner if some of the contacts are sliding as opposed to rolling.

2. The honeycomb lattice in $D = 2$ offers a case in which the rolling kinematics can be exactly solved. The most surprising feature of the result is that the scale of the angular velocities ω grows linearly with the size of the system, although the average of the angular velocity is moderated by the fact that the rotations on two alternating sub-lattices roughly cancel.

3. The dynamics of the honeycomb lattice can also be solved. The conclusion is that the requirement that all normal forces be compressive can only be satisfied for packings smaller than ℓ, with

$$\ell \sim d/I, \tag{77}$$

   where I is the Inertia Number, given by Eq. (3).

4. For random lattices, a Fokker-Planck approximation to the kinetics yields the same key result as for the honeycomb lattice, i.e., that the typical angular velocity grows linearly with the size of a coherently rolling region. Again, the average

angular velocity is much smaller. The presence of odd plaquettes of particles in contact will require compensating sliding contacts even if the coefficient of friction is large; the statistics of these sliding contacts are analogous to those of frustrated bonds in random anti-ferromagnets.

There remains the very interesting question of the nature of the flow for scales larger than ℓ. We can understand the role of ℓ by considering the free volume in the system. For flows in systems of size $L < \ell$, while free volume might be created by collisions generating a granular temperature, such free volume can be removed from the system through the role of inelasticity (or friction) in quenching the granular temperature. On the other hand, for $L > \ell$, free volume must be created and persist in the system, regardless of the quenching effect of inelasticity. It is simply no longer possible for all of the stress-transmitting contacts to have lifetimes $> \dot{\gamma}^{-1}$, consistent with observations of the relatively short duration of most two-particle collisions [13]. Although we have focused on the continuous motion of systems for which $L < \ell$, the fact remains that the chute flow phase diagram, or the results of Alonso-Marroquín mentioned above, emphasize the difficulty of flowing granular systems of size $< \ell$, suggesting that as a practical matter free volume is necessary to achieve a robust flowing state.

I would claim that the rheology of this state, in which free volume plays a significant role, while many neighboring particles also have rotational motions effectively locked to one another, is probably poorly addressed by conventional or modified kinetic theory approaches, due to the presence of long-range correlations in particle motion. The interpretation of the GDR MiDi or Pouliquen flow rule type rheologies in terms of a length scale ℓ obviously disallows such approaches. In this article, I have shown that this length scale ℓ does have a clear physical meaning for $L < \ell$; however, it remains to be seen what aspects of this meaning persist for systems of size $L > \ell$.

Acknowledgments

References

[1] A.N. Schofield and C.P. Wroth, *Critical State Soil Mechanics,* (McGraw-Hill, 1968).

[2] C.K.K. Lun and S.B. Savage, J. Appl. Mech. **54** (1987), 47.

[3] V. Kumaran, J. Fluid Mech **599** (2008), 121; and references therein.

[4] D. Ertaş and T.C. Halsey, Europhys. Letts. **60** (2002), 931; T.C. Halsey and D. Ertaş, arXiv: cond-mat/0506170.

[5] J.T. Jenkins, Phys. Fluids **18** (2006), 103307.

[6] G.D.R. MiDi, Eur. Phys. Journ. E **14** (2004), 341.

[7] O. Baran et al., Phys. Rev. E **74** (2006), 051302.

[8] O. Pouliquen, Phys. of Fluids **11** (1999), 542.

[9] L.E. Silbert et al., Phys. Rev. E **64** (2001), 051302–1.

[10] T. Börzsönyi, T.C. Halsey and R.E. Ecke, Phys. Rev. E **78** (2008), 011306.

[11] R.A. Bagnold, Proc. Roy. Soc. London A, **225** (1954), 49; **295** (1966), 219.

[12] L.E. Silbert, J.W. Landry, and G.S. Grest, Phys. Fluids **15** (2003), 1.

[13] L.E. Silbert, G.S. Grest, R. Brewster, and A.J. Levine, Phys. Rev. Lett. **99** (2007), 068002.

[14] S.F. Edwards, Physica A **249** (1998), 226; S. Alexander, Phys. Rep. **296** (1998), 65.

[15] T.C. Halsey, Phys. Rev. E **80** (2009), 011303.

[16] L. Rothenburg and N.P. Kruyt, Int. J. Solids and Struct., **41** (2004), 5763.

[17] The coefficient of the sliding contact term is slightly different from the force-counting argument in L.E. Silbert, D. Ertaş, G.S. Grest, T.C. Halsey, D. Levine, Phys. Rev. E **65** (2002), 051307, due to the fact that sliding constrains only one kinematical variable (the distance of the centers of the particles), while the force counting at a sliding contact is determined by the criterion of Coulomb yield.

[18] The criterion that a contact be sliding reduces the number of kinematical constraints, but introduces an equivalent number of Coulomb constraints linking T to N, as in T.C. Halsey and D. Ertaş, Phys. Rev. Lett. **83** (1999), 5007.

[19] Traction and dissipation at a rolling contact are treated in K.L. Johnson, *Contact Mechanics*, (Cambridge Univ. Press, Cambridge, 1985) p. 306 ff.

[20] F. Alonso-Marroquín et al., Phys. Rev. E **74** (2006), 031306.

[21] M. Weigel and D. Johnston, Phys. Rev. B **76** (2007), 054408; for a review see R. Moessner, Can. J. Phys. **79** (2001), 1283.

[22] A similar approach, also based on frustration, was used by R.C. Ball and R. Blumenfeld to approach static states and perturbations thereof in R.C. Ball and R. Blumenfeld, Phys. Rev. Lett. **88** (2002), 115505–1; R. Blumenfeld, Physica A **336** (2004), 361.

[23] N. Rivier and D.M. Duffy, J. Phys. C: Solid State Phys. **15** (1982), 2867.